

Cadmium silicate nanopowders for radiation dosimetry application: Luminescence and dielectric studies

B.M. Manohara^{a,b,✉}, H. Nagabhushana^{c,*}, K. Thyagarajan^d, B. Daruka Prasad^{b,e}, S.C. Prashantha^f, S.C. Sharma^g, B.M. Nagabhushana^h

^a Department of Physics, Govt. First Grade College, Davangere 577004, India

^b Jawaharlal Nehru Technological University, Ananthapuram 515002, India

^c Prof. C.N.R. Rao Centre for Advanced Materials, Tumkur University, Tumkur 572103, India

^d Department of Physics, JNTUA College of Engineering, Pulivendula 516390, India

^e Department of Physics, B.M.S. Institute of Technology, Bangalore 560064, India

^f Department of Physics, East West Institute of Technology, Bangalore 560091, India

^g Chhattisgarh Swami Vivekananda Technical University, North Park Avenue, Sector – 8, Bhilai, Chhattisgarh 490009, India

^h Department of Chemistry, M.S. Ramaiah Institute of Technology, Bangalore 560054, India

ARTICLE INFO

Article history:

Received 27 August 2014

Received in revised form 12 January 2015

Accepted 6 February 2015

Available online 26 February 2015

Keywords:

Meso-structured silica

Nanophosphor

Thermoluminescence

Dielectric

ABSTRACT

Pure cadmium silicate (CdSiO_3) nanophosphor was prepared by a low temperature solution combustion technique. In this technique, meso-structured silica was used as silica source. The prepared compounds were well characterized by powder X-ray diffraction (PXRD), scanning electron microscopy, high resolution transmission electron microscopy, Fourier transform infrared and UV-vis spectroscopic techniques. The PXRD peaks of as-formed sample are broad and amorphous in nature. The compound calcined at 800 °C shows pure monoclinic phase, which is the lowest temperature reported so far to obtain in this phase. The average crystallite size for phase pure compound was found to be ~31 nm. The optical energy band gap of ~5.6 eV was observed for the compound. Raman spectrum of the sample showed the all possible states of vibrational motions of the prepared samples. The UV irradiated samples with different dose and time with constant heating rate exhibit the thermoluminescence (TL) with a well resolved glow peak at ~160 °C. The variation of TL intensity with dosage time results that the material was found to be quite useful in radiation dosimetry. The frequency dependent dielectric constant of the prepared sample exhibits high value at low frequency and vice versa.

© 2015 The Ceramic Society of Japan and the Korean Ceramic Society. Production and hosting by Elsevier B.V. All rights reserved.

1. Introduction

Phosphors with highly stable, good morphology and better yield were in great demand for energy saving applications such as display, lasers, scintillators, safety indicators and dosimetry [1,2]. In this regard, rare earth's doped silicates based phosphors exhibit multi-color phosphorescence and are stable against acid, alkali and oxygen environments [3]. Various silicate hosts were well

studied by doping with rare earth and transition metal ions such as $\text{CdSiO}_3:\text{In}^{3+}$, $\text{CdSiO}_3:\text{Mn}^{2+}$, $\text{CdSiO}_3:\text{Sm}^{3+}$, $\text{CdSiO}_3:\text{Tb}^{3+}$, $\text{CaSiO}_3:\text{Eu}^{3+}$, $\text{Ba}_2\text{SiO}_4:\text{Eu}^{2+}$, $\text{Sr}_2\text{SiO}_4:\text{Pr}^{3+}$, $\text{Mg}_2\text{SiO}_4:\text{Tb}^{3+}$, $\text{Zn}_2\text{SiO}_4:\text{Mn}^{2+}$, $\text{Mg}_2\text{SiO}_4:\text{Eu}^{3+}$, $\text{Mg}_2\text{SiO}_4:\text{Dy}^{3+}$, and $\text{Sr}_2\text{SiO}_4:\text{Pr}^{3+}$ [4–13]. Among the various silicates CdSiO_3 as a host exhibits remarkable optical and luminescent properties. Due to the presence of Cd^{2+} ions and strong interaction between Si–O of SiO_3 group, CdSiO_3 shows combined nature of ionic and covalent bonding. The crystal structure of CdSiO_3 shows one dimensional chain of edge-sharing SiO_4 tetrahedron helping in replacing the Cd site by transition metal ions. However in order to maintain the charge neutrality, the charge compensation of Cd^{2+} and O^{2-} was tuned by rare earth ions as a dopant. These dopants were responsible for the creation of traps at appropriate depths, which stores the excitation energy and emit the light in the visible range after some time [14,15].

Thermoluminescence (TL) is a phenomenon of emission of light caused by thermal stimulation by the ionizing radiation on the

* Corresponding author. Tel.: +91 9945954010; fax: +91 8162271924.

** Corresponding author at: Prof. C.N.R. Rao Centre for Advanced Materials, Tumkur University, Tumkur 572103, India. Tel.: +91 9632552517.

E-mail addresses: bmm6627@gmail.com (B.M. Manohara), bhushanlc@gmail.com (H. Nagabhushana).

Peer review under responsibility of The Ceramic Society of Japan and the Korean Ceramic Society.

material induces electrons from the traps of the semiconductors or insulators. A TL glow curve provides the information about the defect centers induced due to ionizing radiations in the material. TL study mainly depends on particle size, type of dopant, morphology, crystallization, growth mechanism, local symmetry, host matrix and synthesis methods. Further, TL finds wide range of applications in the field of archeology, radiation dosimetry and defect studies [16,17]. Therefore, to improve the structural properties of the luminescent materials, the exothermic reaction based solution combustion technique was developed [18]. The reported work in this paper is the first time synthesis of CdSiO₃ nanopowder using oxalyldihydrazide (ODH) as a fuel and meso-structured silica as silica source during solution combustion. The prepared samples were well characterized by powder X-ray diffraction (PXRD), scanning electron microscope (SEM), high resolution transmission electron microscopy (HRTEM), Fourier transform infrared spectroscopy (FTIR) and UV-vis spectroscopy (UV-vis). Thermoluminescence (TL), dielectric and ac conductivity studies were discussed in detail.

2. Experimental

2.1. Synthesis of meso-structured silica

Meso-structured silica was prepared by taking appropriate quantities of hexadecyltrimethyl ammonium bromide (CTAB, Sigma Aldrich), KOH and distilled water. The mixture was heated at 80 °C for 30 min. After uniform mixing of solution for about 30 min, 3.0 mL of tetraethyl orthosilicate (TEOS, Sigma Aldrich) was added to the mixture dropwise under fast stirring to obtain a suspension. The obtained suspension was kept at 80 °C for 2 h to complete the precipitation process. The decomposition of the prepared precipitate was controlled by allowing it to cool at room temperature. Further thoroughly washed with deionised water and dried for 12 h at 80 °C [19].

2.2. Synthesis of CdSiO₃ nanopowder

The materials used for synthesis of CdSiO₃ were cadmium nitrate (Cd(NO₃)₂·4H₂O) and freshly prepared meso-structured silica (Section 2.1) was used as the source of Cd and Si respectively. The stoichiometric quantity of the redox mixture was taken in Petri dish in the ratio of 1:1 and dissolved in deionised water [20]. Then the required amount of ODH was added to the mixture and stirred well for 15–20 min using magnetic stirrer. The mixture was placed in a preheated Muffle furnace maintained at 500 ± 10 °C. The reaction took place within few seconds by heating the redox mixture followed by decomposition. During this process initially large amount of gases (usually CO₂, H₂O and N₂) liberate followed by a spontaneous ignition occurred and then the solution underwent flame type combustion with swelling. After combustion, the product was cooled and grinded well using mortar and pestle. The fine powder was calcined at various temperatures such as 600, 700, 800 and 900 °C for 2 h.

2.3. Measurements

Powder X-ray diffraction (PXRD) analysis was performed using Philips analytical X-ray diffractometer with CuK_α radiation ($\lambda = 1.5405 \text{ \AA}$) along with a nickel filter. The data were collected in 2θ range from 10° to 60°. Morphology of the sample was analyzed by using Hitachi table top scanning electron microscope (SEM – TM 3000). Transmission electron microscopy (TEM), high resolution transmission electron microscopy (HRTEM) and selected-area electron diffraction (SAED) pattern were done using JEOL 2100 HRTEM. Fourier transform infrared (FTIR) spectra were recorded in absorption mode with Perkin Elmer spectrometer (Spectrum

1000) along with KBr pellets. UV-vis spectrum of the sample was recorded with the Elico SL 159 spectrometer by dispersing the powder in liquid paraffin. Raman spectra are recorded on a Raman Horiba Jobin yvon-labram-HR 800 Raman spectrometer in the frequency range of 50–1200 cm⁻¹. For TL studies, samples were exposed to UV-source of wavelength 254 nm and power of 15 W. Samples were filled in the sample holder of squares with area approximately 1 cm² by keeping the distance between the source and sample at constant distance of 1 cm where the intensity was 0.028 W m⁻². The samples were exposed in varied times such as 5–40 min at room temperature (RT). After the desired exposure, the TL glow curves were recorded using Nucleonix TL reader consisting of a small metal planchet (72% Fe, 23% Al and 2% Cr or Nichrome) heated directly using a temperature programmer. During TL measurements, each time ~30 mg of the samples were taken and heating rate was set to 5 °C s⁻¹. Highly polished pellets with a thin layer of silver paste on either side of the pellets (for ohmic contacts) were used for dielectric measurements. Measurements were carried out at room temperature (RT) using LCR meter model HIOKI 3532-50 LCR HiTESTER version 2.3, in the frequency range of 50 Hz–5 MHz.

3. Results and discussion

3.1. Investigations from PXRD

Fig. 1 shows the PXRD patterns of mesoporous silica (Fig. 1(a); JCPDS card No. 47-0715), CdO (Fig. 1(b); JCPDS card No. 78-0653) and CdSiO₃ (Fig. 1(c)–(f)). The diffraction peaks of CdSiO₃ were well matched with the JCPDS card No. 35-0810 [21] confirming the formation of cadmium silicate. Among the prepared silica, the sample calcined at 800 °C for 2 h shows better crystallinity and single monoclinic phase [22–24]. To the best of our knowledge, this is the best possible lowest temperature for the synthesis of

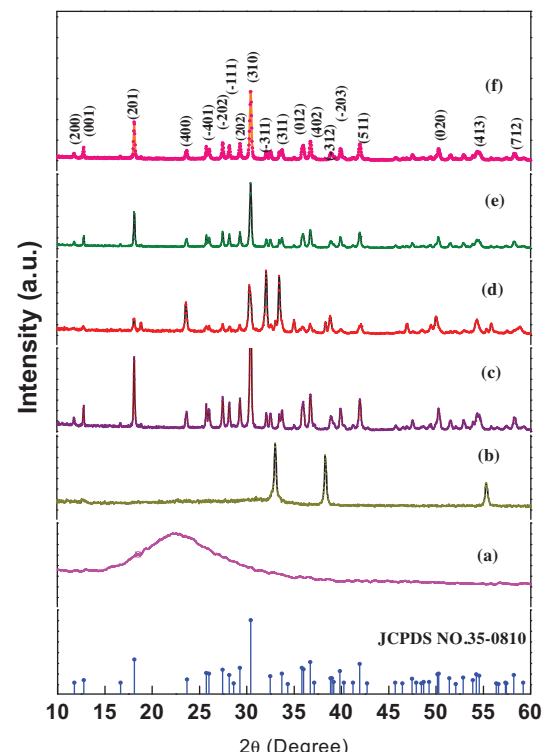


Fig. 1. PXRD of mesoporous silica, CdO and CdSiO₃: (a) mesoporous silica, (b) as formed sample contains CdO and amorphous silica. Further, samples were calcined at (c) 600 °C, (d) 700 °C, (e) 800 °C and (f) 900 °C for 2 h.

CdSiO_3 so far observed in the literature. The average crystallite size was estimated by employing the Debye-Scherrer's formula [25,26].

$$d = \frac{k\lambda}{\beta \cos \theta} \quad (1)$$

where β is the full width at half maximum (FWHM) of the prominent diffraction peaks, ' λ ' is the wavelength of X-ray ($\lambda = 1.5405 \text{ \AA}$) used, ' θ ' is the Bragg's angle and 'k' is the Scherrer's constant. The average crystallite size of the CdSiO_3 sample was found to be $\sim 31 \text{ nm}$ for the samples calcined at 800°C for 2 h. It is known that the FWHM can be expressed as a linear combination of the contribution from the lattice strain and crystalline size [27]. Further, strain present in the CdSiO_3 nanopowder prepared by above-mentioned method was estimated using the Williamson-Hall (W-H) equation.

$$\beta \cos \theta = \frac{k\lambda}{D} + 4\varepsilon \sin \theta \quad (2)$$

where β is the FWHM (in radians), ' θ ' is the Bragg angle of the peak, ' λ ' is the wavelength of X-ray used, 'D' is the effective particle size and ' ε ' is the effective particle size for which

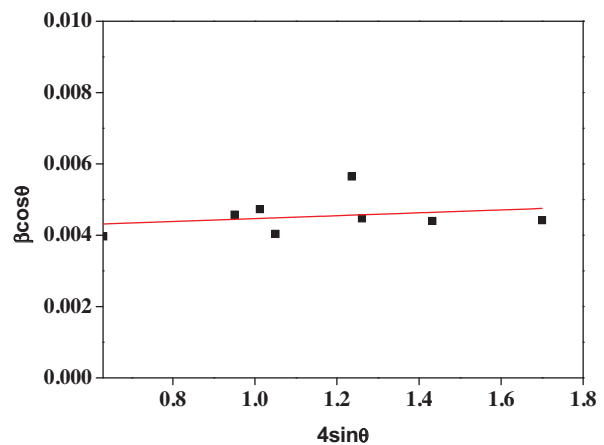


Fig. 2. Williamson-Hall plots of CdSiO_3 nanopowder calcined at 800°C for 2 h.

the strain has been taken into account can be estimated from the extrapolation of the plot as shown in Fig. 2. The average crystallite size estimated from Scherrer's method and W-H plots was well matched with one another.

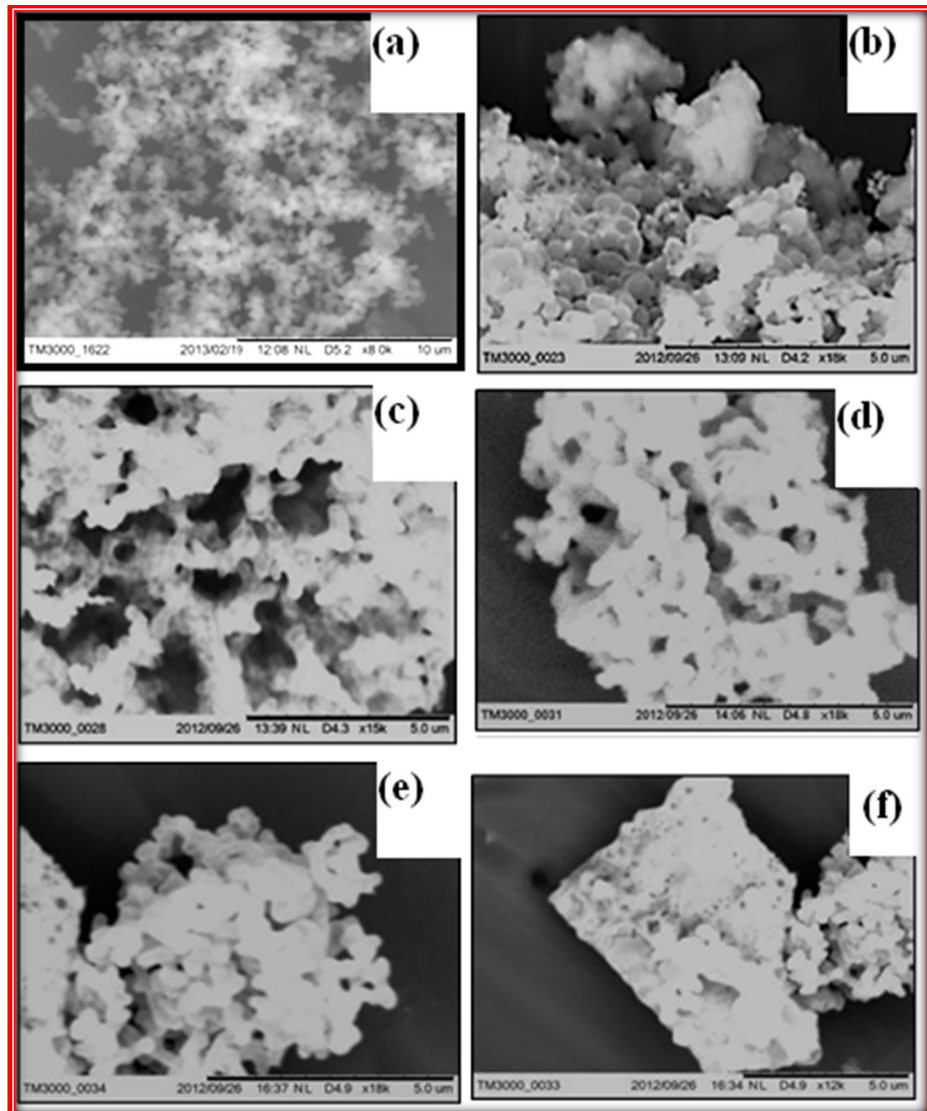


Fig. 3. SEM images of CdSiO_3 nanopowder: (a) CdO and amorphous silica combination (b–f) calcined at (b) 600°C , (c) 700°C , (d) 800°C and (e) 900°C for 2 h.

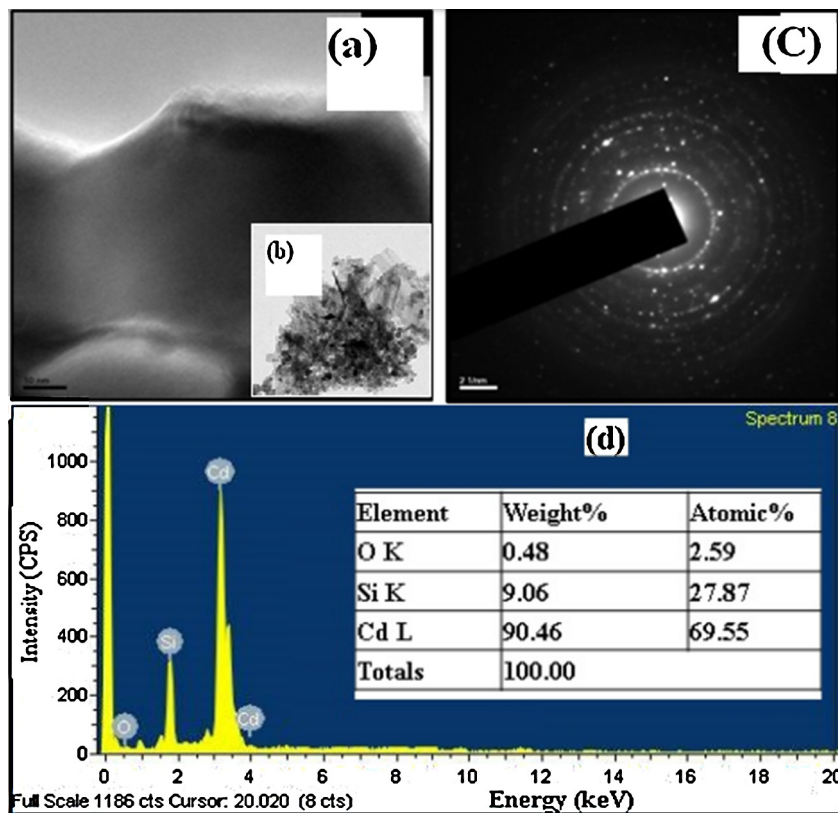


Fig. 4. (a) HRTEM image. (b) TEM image. (c) SAED. (d) EDX of CdSiO_3 nanopowder calcined at 800°C for 2 h.

3.2. Morphological analysis

Transmission and scanning electron microscopes (TEM and SEM) together provide an important tool for the characterization of nano and surface morphologies of the materials. SEM analysis shown in Fig. 3 reveals that the morphology of CdSiO_3 nanopowders was porous and agglomerated with polycrystalline nature. The pores and voids can be attributed to the large amount of gases escaping out of the reaction mixture during combustion. HRTEM and TEM images of CdSiO_3 nanopowder were shown in Fig. 4(a) and (b) respectively. The sample consists of irregular shaped particles with an average particle size of $\sim 30\text{ nm}$. Fig. 4(c) shows the SAED pattern of CdSiO_3 nanopowder having polycrystalline nature. The possible elements present were studied by energy dispersive X-ray analysis (EDAX) shown in Fig. 4(d) and table as a inset of Fig. 4(d) shows quantity of element present in the sample confirming the presence of only Cd, Cu, Si and O elements. The Cu element identified was due to copper grid used as a base material [29,30].

3.3. Fourier transform infrared (FTIR) spectroscopy

In order to investigate the nature of the chemical bonds formed in the prepared sample, FTIR spectra were recorded in the range of $4000\text{--}400\text{ cm}^{-1}$ using Perkin Elmer Spectrum 65 with KBr pellets (Fig. 5). The spectra showing the broad band from 875 to 1114 cm^{-1} was due to asymmetric stretching vibration of $\text{Si}=\text{O}=\text{Si}$ bond and stretching vibrations of terminal $\text{Si}=\text{O}$ bonds. The peaks at 468 cm^{-1} were the characteristic stretching vibrations of $\text{Si}=\text{O}=\text{Si}$ bridges. A weak absorption peak at 2397 cm^{-1} indicating the presence of $\text{C}=\text{O}$ bond in the structure, may be due to adsorbed CO_2 in the sample during FTIR measurements [31,32]. The sharp peak corresponding to $\sim 680\text{ cm}^{-1}$ can be ascribed to $\text{Si}=\text{O}$ bond, which exists in the form of SiO_3 . The absorption at around 3490 cm^{-1} indicates the

presence of hydroxyl groups (surface adsorbed), which is probably due to the fact that the spectra were not recorded in situ which leads to absorption of water from the atmosphere.

3.4. UV-vis spectra investigations

The optical energy gap (E_g) of CdSiO_3 nanopowder calcined at 800°C for 2 h was calculated using Tauc relation [33]. The energy

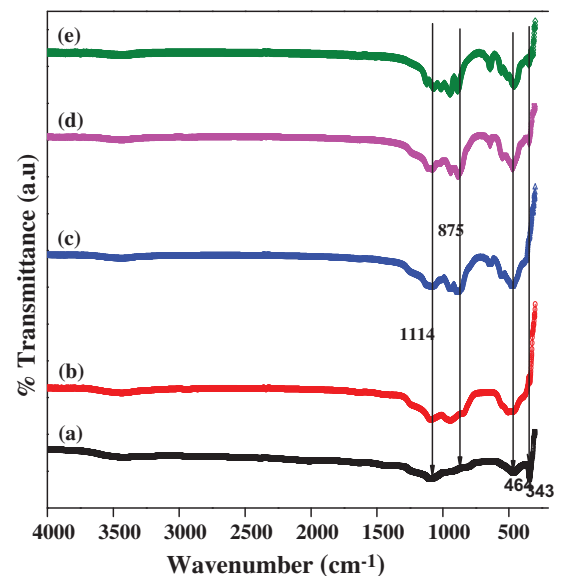


Fig. 5. FTIR of CdSiO_3 nanopowder: (a) as formed and calcined at (b) 600°C , (c) 700°C , (d) 800°C and (e) 900°C for 2 h.

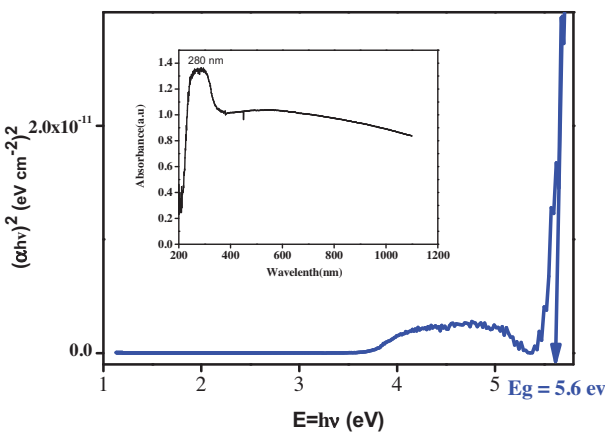


Fig. 6. Energy band gap of CdSiO₃ nanopowder calcined at 800 °C for 2 h (inset: UV-vis absorption spectrum of CdSiO₃ nanopowder).

gap (E_g) has been evaluated for CdSiO₃ nanopowder by fitting absorption data to the direct transition equation

$$(\alpha h c / \lambda) = A \left(\frac{hc}{\lambda} - E_g \right)^n \quad (3)$$

where λ is the wavelength, A is the constant and n can have values 1/2, 3/2, 2 and 3 depending on the mode of inter-band transition, i.e. direct allowed and direct forbidden, indirect allowed and indirect forbidden transitions respectively. Plotting $(\alpha h c / \lambda)^2$ as a function of photon energy (hc/λ) and extrapolating the linear portion of the curve at zero absorption gives the value of the direct band gap (E_g) (Fig. 6). The inset of Fig. 6 shows the UV-vis absorption spectrum taken in the range of 200–1100 nm. The estimated value of E_g is found to be ~5.6 eV.

3.5. Raman spectrum of pure CdSiO₃

The Raman spectrum is widely used to study vibrational, rotational, and other low-frequency modes in a system. The interaction of light with atomic vibrations results in the energy of incident photons being shifted up or down, the energy shift being depending on the spatial derivatives of the macroscopic polarization [34,35]. The Raman spectrum for the sample indicates the presence of prominent and highest vibrational band at 966.7 cm⁻¹ along with two antisymmetric stretching modes appearing at 1006.2 and 1036 cm⁻¹ (Fig. 7). The peak at 1006.3 cm⁻¹ is due to the symmetric stretching mode of the SiO₆ octahedral group; the two lower

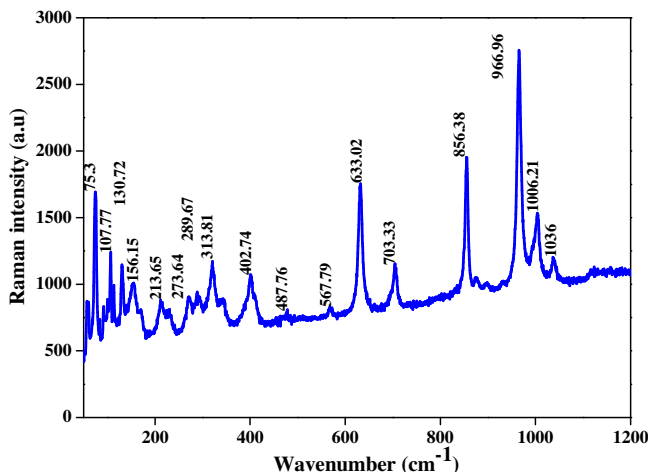


Fig. 7. Raman spectrum of CdSiO₃ in the range 50–1200 cm⁻¹.

Table 1

Raman shifts and their respective matching modes with identical symmetry of CdSiO₃.

Raman shift (cm ⁻¹)	Irreducible representation [36]
130.7	A _u
273.0	B _{2g}
313.8	A _g
402.7	B _{2g}
487.7	A _g
633.0	B _{3g}
703.0	B _{3g}
856.4	B _{3g}
966.9	B _{3g}
1006.0	B _{3g}
1036.0	B _{3g}

frequency modes 633.02 and 856.38 cm⁻¹ are likely to be associated with motion of the cadmium ion. Bands below 350 cm⁻¹ are due to external modes and are difficult to be assigned because of mixing. At 487 cm⁻¹, the Ag mode corresponds to the scissors movement of Si–O–Si groups along the *c* axis, while the peak at 273 and 130.7 cm⁻¹ are due to an A_u and B_{3g} mode related with the bending of O–Si–O groups within the ab plane and the simultaneous movement of Cd ions along the *b* axis. Table 1 lists the band locations for the major Raman bands and shoulders along with other possible modes.

3.6. Thermoluminescence (TL) studies

TL behavior of UV rayed sample was studied in the range of 4.7–38 Gy dose at RT. The dose was calculated by considering the dimensions of the sample holder, the distance of the sample from the UV source, density of the sample filled in the sample holder and the standard parameters like wavelength, power and number of photons emission per second of the used UV bulb. TL glow curves of CdSiO₃ nanopowder and the variations of TL intensity as a function of UV dose (4.7–38 Gy) were shown in Fig. 8 and Fig. 9(a), respectively. TL glow curve shows the increase in intensity with UV dose and a strong peak was observed at ~110–160 °C. The main process of the dissipation of energy absorbed by a material with self-trapped exciton is due to annihilation of self-trapped

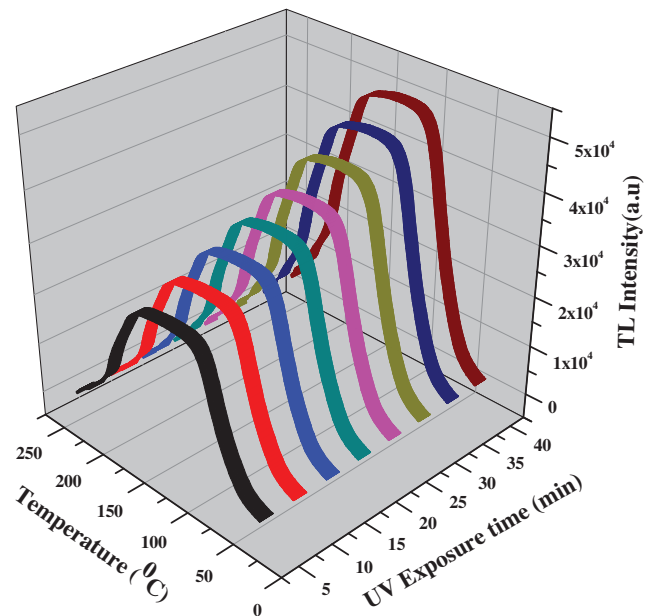


Fig. 8. TL glow curves of UV irradiated CdSiO₃ nanopowder.

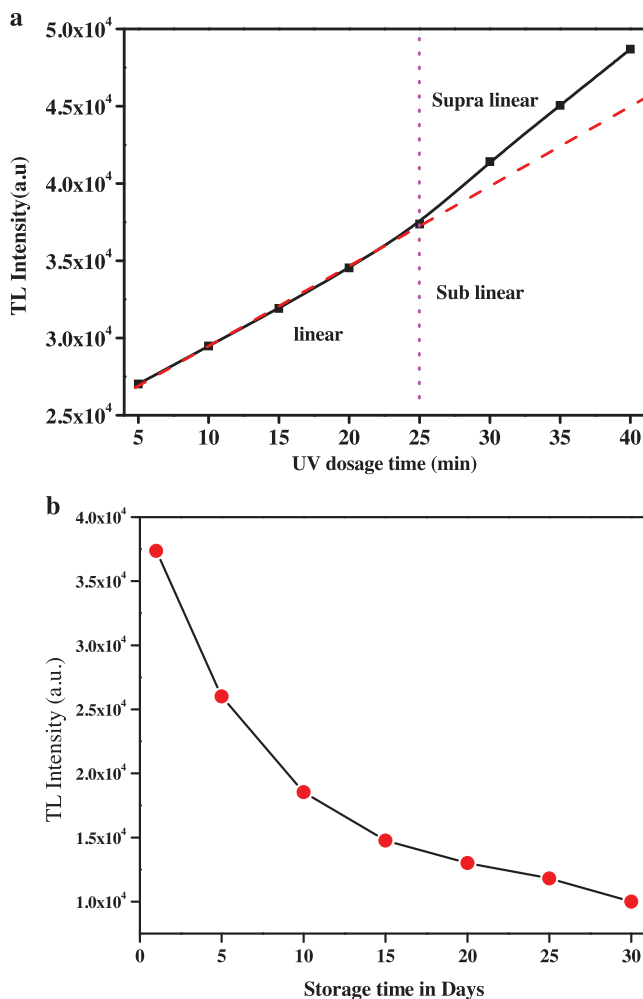


Fig. 9. (a) Variation of TL intensity as a function of UV irradiation dose (5–40 min). (b) Effect of fading with number of days in pure CdSiO_3 nanopowder (25 min UV expose time).

and impurity-trapped excitons. The observed TL peaks may be attributed to recombination of trapped electrons with different holes [37–41].

Fading is the unintentional loss of the TL signal which leads to an underestimation of the absorbed dose. Thermal fading initiates from the fact that even at room temperature there is a cause by optical stimulation. In general, high-sensitivity materials should be handled carefully and stored in opaque containers to prevent fading from light exposure. Other types of fading, which are not temperature dependent, are caused by quantum mechanical tunneling of the trapped charge to recombination sites and transitions between localized states, i.e. transitions that do not take place via the delocalized bands. To study the fading effect, the pure CdSiO_3 was given UV expose for about 25 min. The TL signal was recorded at different intervals of time for nearly 30 days. Fig. 9(b) shows the plot of TL intensity versus the number of days after irradiation. Strong fading was observed after 15 days with the TL signal losing around 62% of its initial value. Subsequently, the signal decayed slowly and finally stabilized after 20 days. The 41% remnant TL signal is high enough to be considered for dosimetric applications [21].

TL glow of the nanopowder might be due to the surface defects. The glow peaks occurred indicate the creation of trapped carriers during irradiation. In nanopowder, most of the ions were at the surface, leading to unsaturated coordinates or easy excitation of electrons or holes. Due to this, the charge carriers are trapped at surface states located in the forbidden gap. During heating process

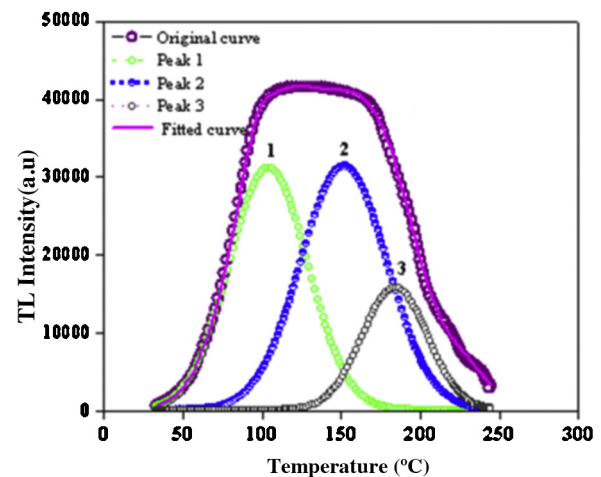


Fig. 10. Glow curve deconvolution of CdSiO_3 nanopowder (UV dose: 30 min).

the recombination of de-trapped electrons and holes emits light. Increase in TL intensity with UV dose is because of more and more traps were getting filled with the increase of absorbed dose and on heating recombination of more and more electrons with holes will release more intense light [42,43].

The dosimetric properties of a material depend mainly on the kinetic parameters responsible for TL. The parameters are activation energy or trap depth (E), the frequency factor (s) and the order of kinetics (b). These parameters will give information about the stability of the traps. If the activation energy is low, then the glow peak occurs at a relatively lower temperature and the corresponding trap is unstable. If it is high, then the trap is relatively stable. The order of kinetics reveals about whether the trapped charge carriers will be retrapped on heating or not. There are several methods present in the literature for the determination of these parameters [44–47]. In the present study the above mentioned parameters were determined by three different standard methods namely Luschik, Halperin–Braner and Chen's method. Glow curve deconvolution of CdSiO_3 nanopowder exposed to UV dose was used for the estimation of kinetic parameters (Table 2). Fig. 10 shows glow curve deconvolution of CdSiO_3 nanopowder (UV dose: 30 min).

The empirical formulae for estimating trapping parameters by Chen's peak shape method [40] are given by

$$E_\alpha = c_\alpha \left(\frac{kT_m^2}{\alpha} \right) - b_\alpha (2kT_m)$$

where with

$$\tau = T_m - T_1, \quad \delta = T_2 - T_m, \quad \omega = T_2 - T_1$$

The order of kinetics (b) or form factor (symmetry factor) ' μ_g ' is given by

$$\mu_g = \frac{T_2 - T_m}{T_2 - T_1} \quad (4)$$

$$\alpha = \tau, \delta, \omega$$

where T_1 and T_2 were calculated, they are the temperatures corresponding to the half of the maximum intensities on either side of the glow peak maximum temperature (T_m). The nature of the kinetics was found by the form factor. Theoretically, the value of geometrical form factor (μ_g) is ~ 0.42 , for first order kinetics and ~ 0.52 for second order kinetics. The ' μ_g ' is found to be practically independent of the activation energy ' E ' and strongly depends on the order of kinetics [41].

Table 2Estimated kinetic parameters using UV irradiated (5–40 min) CdSiO₃ nanopowder.

UV-dose (Gy) exposed to the sample for different times	Peak	<i>T_m</i> (°C)	Balarin parameter (γ)	Order of kinetics, <i>b</i> (μg)	Activation energy (eV)			Frequency factor, <i>s</i> (s^{-1})
					Lushchik method	Halperin–Braner method	Chen's method	
~4.7	1	93.91	0.95	2(0.51)	0.89	0.65	0.72	9.66E+09
	2	131.15	1.09	2(0.48)	0.88	0.57	0.59	1.64E+07
	3	175.58	0.98	2(0.51)	1.33	0.95	1.05	8.41E+11
~9	1	95.91	1.06	2(0.49)	1.71	1.12	1.25	2.4E+17
	2	131.95	1.04	2(0.49)	0.67	0.45	0.46	3.15E+05
	3	174.39	1.05	2(0.49)	2.00	1.34	1.49	9.43E+16
~14	1	94.93	0.97	2(0.51)	1.72	1.25	1.43	9.70E+19
	2	118.46	0.95	2(0.51)	0.69	0.51	0.55	8.47E+06
	3	175.77	1.03	2(0.49)	1.12	0.76	0.82	1.56E+09
~19	1	102.2	0.97	2(0.51)	0.91	0.66	0.73	6.43E+09
	2	135.25	1.00	2(0.50)	1.97	1.38	1.56	4.09E+19
	3	164.74	0.98	2(0.4951)	0.94	0.67	0.73	1.96E+08
~24	1	94.27	1.00	2(0.50)	1.93	1.35	1.54	3.80E+21
	2	117.6	0.99	2(0.50)	0.75	0.26	0.55	1.05E+07
	3	173.86	1.00	2(0.50)	1.18	0.83	0.90	1.45E+10
~28	1	104.18	1.03	2(0.49)	0.89	0.61	0.65	4.83E+08
	2	152.11	1.03	2(0.49)	1.01	0.69	0.74	4.49E+08
	3	184.77	1.08	2(0.48)	1.62	1.05	1.14	4.28E+12
~33	1	104.12	1.03	2(0.49)	0.87	0.59	0.63	2.46E+08
	2	152.11	1.03	2(0.49)	1.01	0.69	0.74	4.49E+08
	3	184.77	1.02	2(0.49)	1.49	1.02	1.12	2.31E+12
~38	1	96.59	1.07	2(0.48)	1.73	1.13	1.25	2.11E+17
	2	131.15	1.00	2(0.50)	0.66	0.46	0.48	5.06E+05
	3	174.65	1.05	2(0.49)	2.12	1.41	1.57	7.53E+17

In the Lushchik method [48], the descending part of the glow peak was used where the area of the half peak, resembled the area of the triangle having identical height and half width. The equation is given by

$$E_\alpha = 2 \left\{ \frac{kT_m^2}{\delta} \right\} \quad (5)$$

In Halperin and Braner [49] method, the ascending part of the glow peak whose area was assumed to be equal to the area of the triangle is given by

$$E_\alpha = 2 \left\{ \frac{kT_m^2}{\tau} \right\} (1 - 3\Delta) \quad (6)$$

where

$$\Delta = 2 \left\{ \frac{kT_m}{E} \right\}$$

In modified Chen's method activation energy is given by [46]

$$E = 3.52 \left\{ \frac{kT_m^2}{\omega - 1} \right\} \quad (7)$$

The equation used for the calculation of frequency factor (*s*) according to Randall and Wilkinson [50] is given by

$$\frac{\beta E}{kT_m^2} = s \exp \left\{ \frac{-E}{kT_m} \right\} Z_m \quad (8)$$

where *k* is the Boltzmann constant and $Z_m = 1 + (b - 1)\Delta_m$.

All the calculated parameters were tabulated in Table 2. The presence of deep traps in CdSiO₃ nanopowder suggests that the sample can be used as a low dose UV radiation dosimeter.

3.7. Dielectric interactions

Few dielectric materials show transient phenomenon on heating followed by irradiation. These phenomena display the same

pattern on behavior for TL, thermally stimulated conductivity (TSC) and exoelectron emission (TSE). These dielectric materials can be used for radiation dosimetry applications. The prepared samples show the insulating behavior based on the energy band gap calculation; hence to check the dielectric behavior the impedance spectroscopy was investigated [51]. Further, this study provides the SiO₃ which can be regarded as probes of the crystal field strength and symmetry in sites occupied by Cd²⁺ ions. The complex dielectric permittivity of the CdSiO₃ is generally

$$\epsilon^* = \epsilon' + i\epsilon'' \quad (9)$$

where ϵ' and ϵ'' are the real and imaginary parts of the complex dielectric permittivity.

The variation of frequency dependent dielectric constant at room temperature is as shown in Figs. 11 and 12. It has been

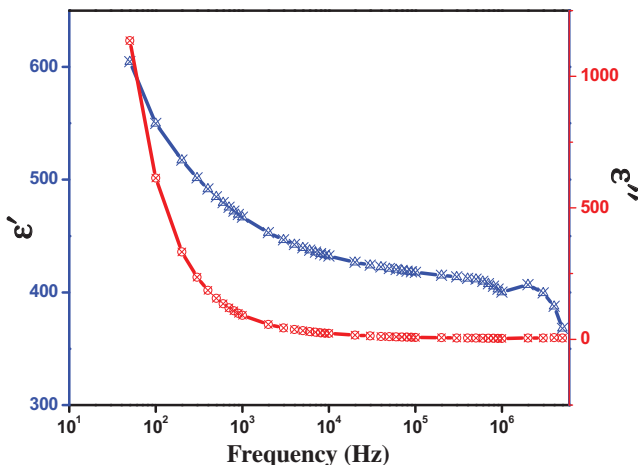


Fig. 11. Variation of real and complex permittivity with frequency at room temperature.

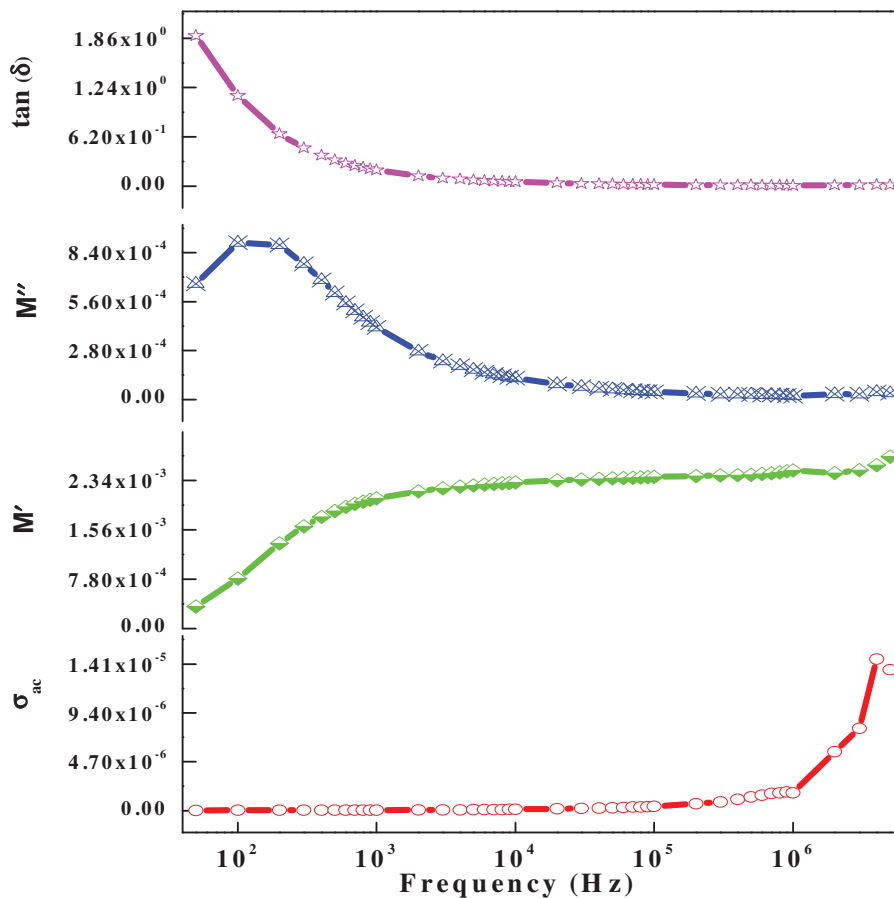


Fig. 12. Variation of $\tan \delta$, ac conductivity and elastic moduli with frequency.

observed that all the samples exhibit the dielectric dispersion where dielectric constant decreases as the frequency increases from 1 Hz to 1 MHz. The decrease in dielectric constant with increasing frequency reaches a constant value and accounts for the fact that beyond a certain frequency, electron hopping cannot follow the alternating field [52]. In view of the fact that mobility of holes is smaller than electrons, the contribution to the polarization from holes is smaller and decreases more rapidly even at lower frequencies than from the later. As a result, the net polarization and dielectric constant decrease.

The values of dielectric constant at lower frequency were found to be about 600–1000 for 100 Hz. The variation in ϵ' was also attributed to the fact that at low frequency regime, the dipolar, interfacial or the surface polarization plays a leading role in determining the dielectric properties of silicates [53]. The higher frequency dielectric constant was attributed to ionic and electronic polarizations that are independent of frequency.

The dielectric loss factor or the dissipation factor is represented as

$$\tan \delta = \frac{\epsilon'}{\epsilon''} \quad (10)$$

Fig. 12 shows the variation of dielectric loss as a function of frequency for the prepared samples. There is a normal trend of dielectric loss without any peaking behavior. It may be due to the fact that the resonance matching may be beyond the analyzed frequency range [54]. Hence there is no power loss due to the transfer of energy from applied field to the oscillating ions within the studied frequency range.

3.8. A.C. conductivity

In order to understand the conduction mechanism, the ac conductivity can be evaluated from the dielectric loss and dielectric permittivity as

$$\sigma_{ac} = \epsilon' \epsilon_0 \omega \tan \delta \quad (11)$$

The variation of ac conductivity of the sample as a function of frequency is as shown in **Fig. 12**. The ac conductivity gradually increases as the frequency of applied field increases. The variation of ac conductivity could be explained in terms of two frequency regions: low frequency and high frequency regions. In low frequency region, grain boundaries are found to be more active so the hopping probability of charge carriers is less whereas, in high frequency region conducting grains are more active promoting the hopping of charge carriers. Probability of charge carriers is less in low frequency region, whereas in high frequency region conducting grains are more active in promoting the hopping of charge carriers. The total conductivity of silicates is:

$$\sigma(\omega, T) = \sigma_{dc}(T) + \sigma_{ac}(\omega, T) \quad (12)$$

where σ_{dc} is the dc conductivity due to band conduction and σ_{ac} is the ac conductivity due to electron hopping between the Cd^{2+} and SiO_3 sites. **Fig. 12** shows the variation of elastic moduli (M' and M'') with frequency supporting the trend of $\tan(\delta)$ variation.

Fig. 13 shows the variations of impedance, resistance and resistivity with frequency. All the terms decreases in their trend with frequency was due to the presence of increased charge carriers like electrons, holes and polarons. The Nyquist plot (**Fig. 14**) for all the compositions shows one overlaid semicircle showing the presence

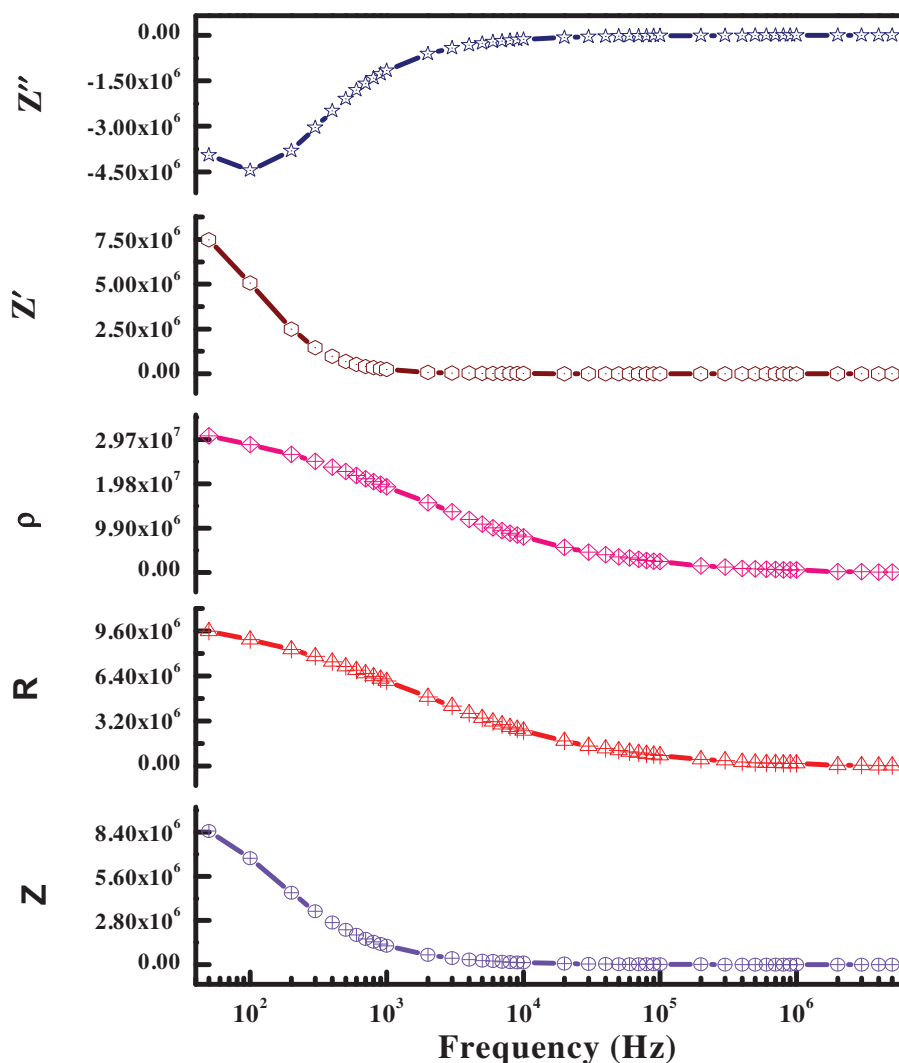


Fig. 13. Variation of impedance and resistance with the frequency.

of single phase with different electrical properties. The higher resistance is attributed to the grain resistance while the lower resistance at lower frequency is attributed to the accumulation of layer resistance. Based on the dielectric behavior and frequency dependent

resistance, the prepared materials are suitable for using it in the low dose radiation dosimeters.

4. Conclusion

For the first time CdSiO_3 nanopowder was successfully synthesized by self sustainable propellant chemistry technique using meso-structured silica as a silica source. PXRD analysis confirms the monoclinic phase and is formed at low calcined temperature of 800°C for 2 h. SEM, TEM and HRTEM images show that the powder was highly porous in nature with lots of voids, foamy and agglomeration. The UV-vis spectra give the energy band gap of $\sim 5.6\text{ eV}$. Single glow peak was seen at 160°C and TL intensity increases linearly with UV dose. Raman spectrum of the sample showed the all possible states of vibrational motions of the prepared samples. This analogy shows important applications in radiation dosimetry. The dielectric dispersion as a function of frequency shows the non-peaking behavior. Due to increased charge carriers, higher conductivity was observed at higher frequency. The CdSiO_3 system shows the high resistance attributed to both grain and grain boundary contributions respectively. The single semicircle of Nyquist plot supports for the single phase of the compound matches with the PXRD results. Hence a simple method of preparation of CdSiO_3 may be the better material for luminescent and low dose radiation dosimeters.

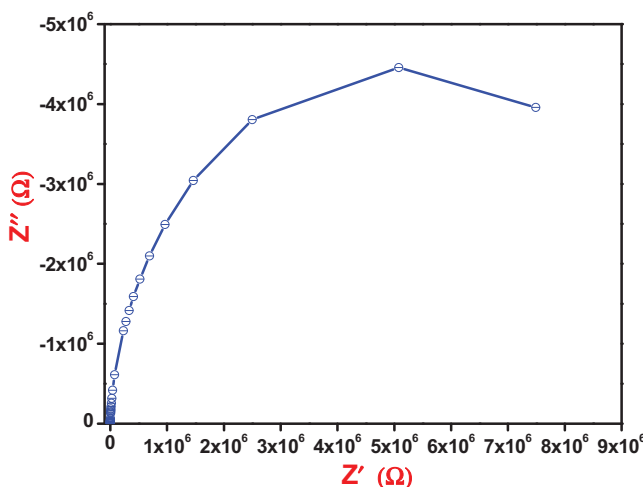


Fig. 14. The complex impedance as a Nyquist plot for CdSiO_3 nanopowder.

Acknowledgements

The author B.M. Manohara is grateful to the Principal and the Head of the Department of Physics, Govt. First Grade College, Davangere, for his constant support and encouragement. The author BMM acknowledges UGC (Project No. MRP/12TH PLAN/14-15/KAD008), New Delhi for sanction of the Project and extends special gratitude to Prof. C.N.R. Rao Centre for Advanced Materials, Tumkur University, Tumkur 572103, India for extending lab facilities.

References

- [1] L.C. Rodrigues, J. Holsa, M. Lastusaari, M.C.F.C. Feinto and H.F. Brito, *J. Mater. Chem. C*, **2**, 1612–1618 (2014).
- [2] B.F. Lei, B. Li, X.J. Wang and W.L. Li, *J. Lumin.*, **118**, 173–178 (2006).
- [3] L. Zhang, G.Y. Hong and X.L. Sun, *Chin. Chem. Lett.*, **10**, 799–802 (1999).
- [4] M. Wang, X. Zhang, Z. Hao, X. Ren, Y. Luo, X. Wang and J. Zhang, *Opt. Mater.*, **32**, 1042–1045 (2010).
- [5] L. Zhang, X. Zhou, H. Zeng, H. Chen and X. Dong, *Mater. Lett.*, **62**, 2539–2541 (2008).
- [6] C. Bull and G.F.J. Garlick, *J. Electrochem. Soc.*, **93**, 371–375 (1951).
- [7] K.J. Yong and L.Y. Liang, *Chin. Phys. Lett.*, **23**, 204–206 (2006).
- [8] B.F. Lei, Y.L. Liu, J. Liu, Z.R. Ye and C.S. Shi, *J. Solid State Chem.*, **177**, 1333–1337 (2004).
- [9] L.C.V. Rodrigues, H.F. Brito, J. Holsa, R. Stefani, M.C.F.C. Felinto, M. Lastusaari, T. Laamanen and L.A.O. Nunes, *J. Phys. Chem. C*, **116**, 11232–11240 (2012).
- [10] R. Kršmanović, Z. Antić, I. Žeković and M.D. Dramicanin, *J. Alloys Compd.*, **480**, 494–498 (2009).
- [11] J.K. Park, *Appl. Phys. Lett.*, **84**, 1647–1649 (2004).
- [12] L. Lin, C. Shi, Z. Wang, W. Zhang and M. Yin, *J. Alloys Compd.*, **466**, 546–550 (2008).
- [13] L. Yang, M. Fang, L. Du, Z. Zhang, L. Ren and X. Yu, *Mater. Res. Bull.*, **43**, 2538–2543 (2008).
- [14] C.A. Barboza, J.M. Henriques, E.L. Albuquerque, E.W.S. Caetano, V.N. Freire and L.A.O. da Costa, *Chem. Phys. Lett.*, **480**, 273–277 (2009).
- [15] B. Lei, Y. Liu, G. Tang, Z. Ye and C. Shi, *Mater. Chem. Phys.*, **87**, 227–232 (2004).
- [16] K.C. Patil, S.T. Aruna and S. Ekambaram, *Curr. Opin. Solid State Mater. Sci.*, **457**, 158–165 (1997).
- [17] C. Manjunatha, D.V. Sunitha, H. Nagabhushana, S.C. Sharma, S. Ashoka, J.L. Rao, B.M. Nagabhushana and R.P.S. Chakradhar, *Mater. Res. Bull.*, **47**, 2306–2314 (2012).
- [18] K.C. Patil, M.S. Hegde, T. Rattan and S.T. Aruna, *Chemistry of Nanocrystalline Oxide Materials, Combustion Synthesis, Properties and Applications*, World Scientific Publishing Co. Pvt. Ltd., Singapore (2008).
- [19] L.P. Santana, E.S. de Almeida, J.L. Soares and F.M. Vichi, *Braz. Chem. Soc.*, **22**, 2013–2017 (2011).
- [20] S.R. Jain, K.C. Adiga and V.R. Paiverneker, *Combust. Flame*, **40**, 71–79 (1981).
- [21] D.V. Sunitha, C. Manjunatha, C.J. Shilpa, H. Nagabhushana, S.C. Sharma, B.M. Nagabhushana, N. Dhananjaya, C. Shivakumara and R.P.S. Chakradhar, *Spectrochim. Acta A: Mol. Biomol. Spectrosc.*, **99**, 279–287 (2012).
- [22] B. Lei, Y. Liu, Z. Ye and C. Shi, *J. Lumin.*, **109**, 215–219 (2004).
- [23] J. Kuang and Y. Liu, *Chem. Phys. Lett.*, **424**, 58–62 (2006).
- [24] C.M. Abreu, R.S. Silva, M.E.G. Valerio and Z.S. Macedo, *J. Solid State Chem.*, **200**, 54–59 (2013).
- [25] X. Qu, L. Cao, W. Liu, G. Su, H. Qu, C. Xu and P. Wang, *J. Alloys Compd.*, **494**, 196–198 (2010).
- [26] Y.L. Liu, J.Y. Kuang, B.F. Lei and C.S. Shi, *J. Mater. Chem.*, **15**, 4025–4031 (2005).
- [27] H.P. Klug and L.E. Alexander, *X-ray Diffraction Procedures: For Polycrystalline and Amorphous Materials*, 2nd ed., Wiley-VCH (1974).
- [28] S.C. Prashantha, B.N. Lakshminarasappa and F. Singh, *J. Lumin.*, **132**, 3093–3097 (2012).
- [29] S.B. Oadri, J.P. Yang, E.F. Skelton and B.R. Ratna, *Appl. Phys. Lett.*, **70**, 1020–1021 (1997).
- [30] G.K. Williamson and W.H. Hall, *Acta Metall.*, **1**, 22–31 (1953).
- [31] D.V. Sunitha, H. Nagabhushana, S.C. Sharma, F. Singh, B.M. Nagabhushana, N. Dhananjaya, C. Shivakumara and R.P.S. Chakradhar, *J. Lumin.*, **143**, 409–417 (2013).
- [32] N. Dhananjaya, H. Nagabhushanan, B.M. Nagabhushana, B. Rudraswamy, C. Shivakumara, K.P. Ramesh and R.P.S. Chakradhar, *Physica B*, **406**, 1645–1652 (2011).
- [33] R.P.S. Chakradar, B.M. Nagabhushana, G.T. Chandrappa, K.P. Ramesh and J.L. Rao, *J. Chem. Phys.*, **121**, 10250 (2004).
- [34] Q. Williams, E. Knittle and R. Jeanloz, *Geophys. Monogr. Ser.*, **45**, 1–12 (1989).
- [35] E. Moreira, J.M. Henriques, D.L. Azevedo, E.W.S. Caetano, V.N. Freire and E.L. Albuquerque, *J. Solid State Chem.*, **184**, 921–928 (2011).
- [36] D.M. Többens and V. Kahlenberg, *Vib. Spectrosc.*, **56**, 265–272 (2011).
- [37] S. Atalay, H.I. Adiguzel and F. Atalay, *Mater. Sci. Eng. A*, **304–306**, 796–799 (2001).
- [38] J. Tauc, R. Grigorovici and A. Vancu, *Phys. Stat. Sol.*, **15**, 627–637 (1966).
- [39] N. Suriyamurthy and B.S. Panigrahi, *J. Lumin.*, **128**, 1809–1814 (2008).
- [40] R. Chen and S.W.S. McKeever, *Theory of Thermoluminescence and Related Phenomena*, World Scientific, Singapore (1997).
- [41] B.M. Manohara, H. Nagabhushana, D.V. Sunitha, K. Thyagarajan, B. Daruka Prasad, S.C. Sharma, B.M. Nagabhushana and R.P.S. Chakradhar, *J. Alloys Compd.*, **592**, 319–327 (2014).
- [42] G. Kitis, C. Furetta, M. Prokic and V. Prokic, *J. Phys. D: Appl. Phys.*, **33**, 1252–1262 (2000).
- [43] M.E. Haghiri, E. Saion, W.S. wan Abdullah, N. Soltani, M. Hashim, M. Navasery and M.A. Shafaei, *Radiat. Phys. Chem.*, **90**, 1–5 (2013).
- [44] R. Sharma, D.P. Bisen, S.J. Dhoble and N. Brahme, *J. Lumin.*, **131**, 2089–2092 (2011).
- [45] O. Annalakshmi, M.T. Jose, U. Madhusoodanan, B. Venkatraman and G. Amarendra, *J. Lumin.*, **141**, 60–66 (2013).
- [46] R. Chen, *J. Electrochem. Soc.*, **116**, 1254–1257 (1969).
- [47] V. Singh, T.K. Gundu Rao and J.-J. Zhu, *J. Lumin.*, **126**, 1–6 (2007).
- [48] C.B. Lushchik, *Sov. Phys. JETP*, **3**, 390–399 (1956).
- [49] A. Halperin and A. Brainer, *Appl. Phys. Rev.*, **117**, 408–415 (1960).
- [50] J.T. Randall and M.H.F. Wilkins, *Proc. Roy. Soc. (Lond.) Ser. A*, **184**, 347–364 (1945).
- [51] C. Bowlt, *Contemp. Phys.*, **17**, 5 (1976).
- [52] P. Kumar, S.K. Sharma, M. Knobel and M. Singh, *J. Alloys Compd.*, **508**, 115–118 (2010).
- [53] B. Daruka Prasad, H. Nagabhushana, K. Thyagarajan, B.M. Nagabhushana, D.M. Jnaneswara, S.C. Sharma, C. Shivakumara, N.O. Gopal, S.-C. Ke and R.P.S. Chakradhar, *J. Alloys Compd.*, **590**, 184–192 (2014).
- [54] M. Hashim, S. Kumar, S.E. Shirath, E.M. Mohammed, H. Chung and R. Kumar, *Physics B: Condens. Matter*, **407**, 4097–4103 (2012).